

# Non-binary dynamical Ising machines for combinatorial optimization

Aditya Shukla, Mikhail Erementchouk and Pinaki Mazumder

Electrical Engineering and Computer Science Department, University of Michigan, Ann Arbor, 48109, MI, U.S.A.

\*Corresponding author(s). E-mail(s): [aditshuk@umich.edu](mailto:aditshuk@umich.edu);  
[merement@gmail.com](mailto:merement@gmail.com);

Contributing authors: [pinakimazum@gmail.com](mailto:pinakimazum@gmail.com);

## Abstract

Dynamical Ising machines achieve accelerated solving of complex combinatorial optimization problems by remapping the convergence to the ground state of the classical spin networks to the evolution of specially constructed continuous dynamical systems. The main adapted principle of constructing such systems is based on requiring that, on the one hand, the system converges to a binary state and, on the other hand, the system's energy in such states mimics the classical Ising Hamiltonian. The emergence of binary-like states is regarded to be an indispensable feature of dynamical Ising machines as it establishes the relation between the machine's continuous terminal state and the inherently discrete solution of a combinatorial optimization problem. This is emphasized by problems where the unknown quantities are represented by spin complexes, for example, the graph coloring problem. In such cases, an imprecise mapping of the continuous states to spin configurations may lead to invalid solutions requiring intensive post-processing. In contrast to such an approach, we show that there exists a class of non-binary dynamical Ising machines without the incongruity between the continuous character of the machine's states and the discreteness of the spin states. We demonstrate this feature by applying such a machine to the problems of finding proper graph coloring, constructing Latin squares, and solving Sudoku puzzles. Thus, we demonstrate that the information characterizing discrete states can be unambiguously presented in essentially continuous dynamical systems. This opens new opportunities in the realization of scalable electronic accelerators of combinatorial optimization.

**Keywords:** combinatorial optimization, graph coloring, Ising machines, quadratic unconstrained binary optimization, Latin squares

# 1 Introduction

The ever-growing demand for solving complex computational problems compels researchers to explore alternative models of computation based on unconventional principles. Recently, the approach employing classical spin systems started attracting explosive interest. The computational capabilities of such systems were a focus of investigations for a long time owing to the relation between the spin states delivering the lowest energy of the Ising model [1–4], and a broad class of combinatorial optimization problems [5,6]. The novel perspective that motivates the special interest is the realization of the computational capabilities of classical spin systems in continuous dynamical systems, which led to the recognition of a particular class of computing devices, the dynamical Ising machines [7–9]. While based on different underlying dynamical principles, from degenerate optical parametric oscillators [10] to bistable dynamics [11], the dynamical Ising machines share a common operational principle. They employ a characteristic feature of selected continuous dynamical systems to converge to binary or close-to-binary states [12]. Ensuring that the energy of such states reproduces the energy of the classical Ising model and that the energy decreases with the machine evolution establishes the connection between the progression of the dynamical Ising machines and finding the ground state of a classical spin system.

A strong binary structure may appear imperative for the terminal states of the Ising machine. Indeed, substantial deviations from such a structure introduce an uncertainty in the correspondence between the machine’s terminal state and the required binary state. In some situations, this uncertainty does not constitute a fundamental challenge. When any binary state represents a solution to an optimization problem, a “suboptimal” mapping of an unstructured terminal state to a binary state only impacts the quality of the solution. From a practical perspective, the quality of the solution is an important metric, but it is only one of the metrics characterizing an approach to solving an optimization problem. If other metrics, such as time complexity, scalability, and parallelizability, are favorable, the approach may still be highly beneficial. However, in some situations, only selected binary states may represent a solution. For example, while solving a coloring (labeling) problem, colors are represented by spin complexes. Not all states of those complexes may correspond to a valid color. From the perspective of the original problem, this means that the “suboptimal” mapping may produce no solution at all, which raises doubt about whether the approach is a viable option for solving high-level optimization problems. It must be noted in this regard that the convergence to a binary state does not eliminate the problem of unfeasible solutions.

In this paper, we present a dynamical Ising machine that goes against the common wisdom. The machine does not necessarily converge to a binary state and, therefore, is non-binary. Yet, the machine’s terminal states trivially produce binary states and do not produce unfeasible solutions for labeling problems. We demonstrate these features of the presented Ising machine for the example of finding Latin squares and solving the Sudoku puzzles, the problems that can be straightforwardly represented as coloring problems. Besides opening a new direction in developing dynamical Ising machines, the presented machine gives a nontrivial example of how binary information can be carried by continuous dynamical systems.

## 2 $V_2$ model

Most modern dynamical Ising machines traverse a continuous spin-space as they dynamically evolve in such a way that they only settle in states where all spins are binary or binary with some marginal error [13–16]. For example, in [11, 17], the convergence to a binary state is enforced by imposing bi-stability on the spins. The design choice for binary terminal states is justified by the equivalence of the designed machine’s Hamiltonian in such states and the Ising Hamiltonian. At the same time, it is now known that a strong bi-stability can severely affect the Ising machines’ performance [18, 19], which makes unclear the practical quality of solutions produced by the Ising machines

This work aims to revisit the notion of whether continuous spins, as internal variables of Ising machines, need to converge to binary values at all, and, consequently, to identify dynamical continuous-spin systems that can solve inherently discrete problems without converging to binary states.

The problem native to the Ising machines is the max-cut problem: finding partitioning a graph with the maximum total weight of edges between the parts. For a given connected graph  $\mathcal{G} = (\mathcal{V}, \mathcal{E})$  with  $N = |\mathcal{V}|$  nodes and weighted adjacency matrix  $A$ , the partition is described by a binary function (spin configuration)  $\boldsymbol{\sigma} : \mathcal{V} \rightarrow \{-1, 1\}$ , or, in other words, by assigning to each graph node  $i \in \mathcal{V}$  a binary variable  $\sigma_i \in \{-1, 1\}$ . Then the max-cut problem can be expressed as

$$\max_{\boldsymbol{\sigma}} C(\boldsymbol{\sigma}) = \max_{\boldsymbol{\sigma}} \left( \frac{1}{4} \sum_{i,j=1}^N A_{i,j} (1 - \sigma_i \sigma_j) \right), \quad (1)$$

where  $C(\boldsymbol{\sigma})$  is discrete cut function defined over a partition of the vertices of  $\mathcal{G}$ . The relation with the classical Ising model is established by presenting  $C(\boldsymbol{\sigma}) = W/2 - H(\boldsymbol{\sigma})/2$ , where  $W = \sum_{i,j} A_{i,j}/2$  is the total weight of the graph edges and  $H(\boldsymbol{\sigma}) = \boldsymbol{\sigma}^T \hat{A} \boldsymbol{\sigma} / 2 = \sum_{i,j} A_{i,j} \sigma_i \sigma_j / 2$  has the meaning of the Hamiltonian of the antiferromagnetic Ising model on graph  $\mathcal{G}$ .

To identify the dynamics governing the non-binary Ising machines, we reformulate the max-cut problem in the spirit of the rank-2 SDP relaxation [20, 21]: in terms of a continuous system of variables  $\boldsymbol{\xi} = \{\xi_1, \dots, \xi_N\}$ , and a respective relaxed continuous cut function  $C_R(\boldsymbol{\xi}) : \mathbb{R}^N \rightarrow \mathbb{R}$ . The connection with the relaxed problem proposed in this work is established by first formulating the partition delivering the max-cut as

$$\boldsymbol{\sigma}' = \arg \max_{\boldsymbol{\sigma}} \left( \frac{1}{2} \sum_{i,j} A_{i,j} \Phi_I(\sigma_i - \sigma_j) \right), \quad (2)$$

where  $\Phi_I(x) = x^2/4$  is the indicator function for the edge between the nodes  $i$  and  $j$  to be cut such that  $\Phi_I(0) = 0$  and  $\Phi_I(\pm 2) = 1$ . Letting the spins (and consequently the cut) to assume continuous values leads to the following class of relaxations of the

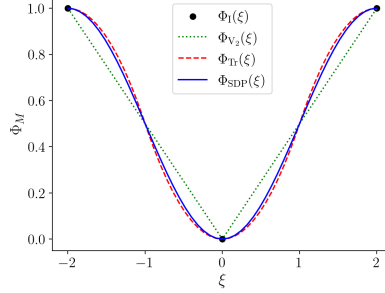


**Fig. 1** Examples of cut-counting functions:  $\Phi_I$  is the discrete function of the binary Ising model,  $\Phi_R(\xi)$  are relaxed functions with  $M = \text{SDP}, \text{Tr}, \text{V}_2$  corresponding to rank-2 SDP relaxation [21], the triangular model from Refs. [16, 22], and the  $\text{V}_2$  model considered in the present paper. For the relaxed cut-counting functions, only one period is shown.

max-cut problem for  $\mathcal{G}$ :

$$\xi' = \arg \max_{\xi} C_R(\xi) = \arg \max_{\xi} \sum_{i,j} A_{i,j} \Phi_R(\xi_i - \xi_j). \quad (3)$$

The relaxed cut-counting function  $\Phi_R(\xi)$  is a periodic function with period 4 constrained by  $\Phi_R(0) = 0$  and  $\Phi_R(\pm 2) = 1$ . A few examples of such functions are shown in Fig. 1. We note that, in addition to the period translations  $\xi_i \rightarrow \xi_i + 4k_i$ , the relaxed cut function  $C_R(\xi)$  is invariant with respect to homogeneous translations  $\xi_i \rightarrow \xi_i + \Delta\xi$ .

The solution to the relaxed problem (3),  $\xi'$ , is not necessarily binary. For example, Eq. (3) with  $\Phi_R(\xi) = \Phi_{\text{SDP}}(\xi) = (1 - \cos(\pi\xi/2))/2$  is equivalent to a rank-2 SDP, which outputs a binary vector only for a special set of graphs e.g. bipartite graphs [21]. For this reason, a rounding procedure is required to map  $\xi'$  to a strictly binary vector. A straightforward approach is a parametric rounding procedure [21–23], which compares with 0 each  $\xi'_i - r$ , where  $r$  is the rounding center, taken by modulo of the period of  $\Phi_R(\xi)$ . This defines rounding as the mapping  $\xi' \mapsto \sigma(r)$ . Generally, this procedure produces a spectrum of rounded configurations  $\sigma(r)$  depending on the value of the rounding center and the respective spectrum of cuts  $C(\sigma(r))$ . Hence, a methodology to find the optimal solution to the rounding problem must accompany solving Eq. (3).

Next, we introduce an important relaxed spin representation [24], which partitions dynamical variables  $\xi_i$  into two components: spin  $\sigma_i \in \pm 1$  and a continuous remainder  $X_i \in [-1, 1)$  according to

$$\xi_i = \sigma_i + X_i + 4k_i, \quad (4)$$

where  $k_i$  is an integer, and 4 represents the period of  $\Phi_R(\xi)$ . Thus, the vector  $\xi = \{\xi_i\}$  is replaced by the vector of pairs  $(\sigma, \mathbf{X}) = \{(\sigma_i, X_i)\}$ .

Assuming that the relaxed cut-counting function possesses the gliding symmetry,  $\Phi_R(\xi + 2) = 1 - \Phi_R(\xi)$ , as all functions shown in Fig. 1 do, the relaxed cut function can be written as [24]

$$C_R(\xi) = C_R(\sigma, \mathbf{X}) = C(\sigma) + \tilde{C}_R(\sigma, \mathbf{X}), \quad (5)$$

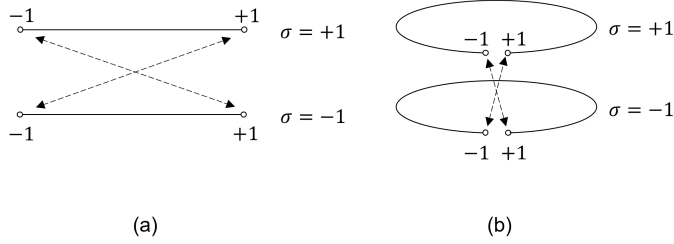


**Fig. 2** The phase space of the dynamical variables in the  $V_2$  model is a wedge sum of two circles with a circumference of 2. (a) Range of a state-vector element  $(\sigma, X)$ , with  $X$  depicted as an open interval. (b)  $(\sigma, X)$  with  $X$  shown as a circle to visualize the continuity of the transition between states  $(\sigma, \pm 1)$  and  $(-\sigma, \mp 1)$ .

where

$$\tilde{C}_R(\boldsymbol{\sigma}, \mathbf{X}) = \frac{1}{4} \sum_{i,j} A_{i,j} \sigma_i \sigma_j \Phi_R(X_i - X_j). \quad (6)$$

Respectively, the equations of motion governing the  $V_2$  Ising machine,  $\dot{\mathbf{X}} = \nabla_{\mathbf{X}} C_R(\boldsymbol{\sigma}, \mathbf{X})$ , have the form

$$\dot{X}_i = \frac{1}{2} \sum_j A_{i,j} \sigma_i \sigma_j \phi_R(X_i - X_j), \quad (7)$$

where  $\phi_R(X) = d\Phi_R(X)/dX$ . At  $X = \pm 1$ , the evolution of  $X$  itself is discontinuous, as illustrated by Fig. 2. The evolution of  $\sigma$  stems from these discontinuous transitions of  $X$ : whenever  $X_m$  crosses the  $X = \pm 1$  boundary,  $\sigma$  changes sign.

From the rounding perspective,  $\boldsymbol{\sigma}$  entering representation (4) can be regarded as rounding of  $\boldsymbol{\xi}$  with respect to a particular choice of the rounding center. Thus, generally, finding the terminal states of the dynamics governed by Eq. (7) should be followed by solving the optimal rounding problem. However, in [24], it was found that this problem is eliminated for the model driven by

$$\phi_V(X) = \frac{1}{2} \text{sgn}(X), \quad (8)$$

where  $\text{sgn}(X)$  is the sign function. Owing to the shape of the plot  $\Phi_V(X) = |X|/2$ , the dynamics described by  $\phi_V(\xi)$  is dubbed the  $V_2$  model, and the Ising machine based on the dynamics is called the  $V_2$ -machine. The  $V_2$  model possesses several key properties, which collectively summarize its behavior as a self-contained dynamical Ising machine. Their proofs and some other general properties of the  $V_2$  model are provided in [24].

First, as the system progresses from an arbitrary initial state, relaxed cut  $C_R$  approaches the canonical discrete cut  $C$  at the steady state. It can be shown that at any point of time,

$$C_V(\boldsymbol{\sigma}, \mathbf{X}) = C(\boldsymbol{\sigma}) + \frac{1}{4} \sum_{i,j} A_{i,j} \sigma_i \sigma_j |X_i - X_j|, \quad (9)$$

and that at the steady state,  $C_R(\boldsymbol{\sigma}, \mathbf{X})$  depends on  $\boldsymbol{\sigma}$  only while any dependence on  $\mathbf{X}$  vanishes.

Second, starting from an arbitrary initial state, the  $V_2$ -machine evolves so that the cut does not decrease with time. As time progresses, the cut represented by the binary component  $\boldsymbol{\sigma}$  does not decrease:

$$C(\boldsymbol{\sigma}(t_2)) \geq C(\boldsymbol{\sigma}(t_1)) \quad (10)$$

for  $t_2 > t_1$ . Equivalently, any evolution following weak perturbations from a steady state does not decrease discrete cut  $C$ .

Finally, it was shown in [24] that the terminal state of the  $V_2$ -machine does not require finding the optimal rounding. While solving the rounding problem,  $\xi_i - r = \sigma_i(r) + X_i(r) + 4k_i(r)$ , may result in different binary configurations  $\boldsymbol{\sigma}(r)$  depending on the rounding center, the cut produced by these configurations has the same weight. Combining with the two properties above, this implies that starting from an arbitrary state  $\boldsymbol{\xi}(0)$ , the  $V_2$ -machine ends up in such state  $(\boldsymbol{\sigma}, \mathbf{X})$  that  $\boldsymbol{\sigma}$  produces a cut not worse than that obtained by the optimal rounding of  $\boldsymbol{\xi}(0)$ .

These properties yield dynamics with an ever-accessible solution to the max-cut problem, whose quality may be further improved with slight but regular perturbation. It must be emphasized that these properties are specific for the  $V_2$  model. For example, for other relaxations shown in Fig. 1,  $\Phi_{\text{SDP}}$  and  $\Phi_{\text{Tr}}$ , the respective discrete component  $\boldsymbol{\sigma}$  does not necessarily hold the best binary state and optimal rounding requires solving a disparate optimization problem [21, 22].

### 3 Graph coloring and stable definite color states

The max-cut problem has the benefit of a relatively straightforward connection with the dynamical models governing Ising machines. In other words, it can be regarded as native to Ising machines. Consequently, applying Ising machines to solving high-level problems requires representing the original problem in terms of graph partitioning. From the theoretical perspective, the sole existence of such representation is warranted by the NP-completeness of the max-cut problem as the decision problem about the existence of cut with the given weight [25]. However, this does not address the practical concerns about finding such representation and making it efficient.

One of the origins of the arising difficulties is the very mapping of high-level variables of the original problem to binary spins within the framework of interacting spin networks. In this case, the original variables are represented by several spins (spin complexes), and, in addition to providing good quality solutions, it is imperative that individual spin complexes converge to states corresponding to valid values of the high-level variables. However, *a priori*, it is not evident that a continuous-spin network governed by particular equations of motion will converge to such states starting from generic initial conditions. For the example of the graph coloring problem considered in detail below, this is illustrated by Fig. 3, which shows the probability of convergence of several Ising machines to a state describing a valid color for a graph with a single node. For each machine, the probability is estimated by restarting the machine 5000 times and counting the number of instances when the machine terminated at a state

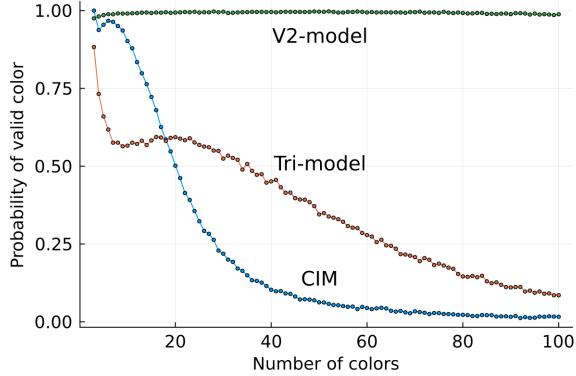


**Fig. 3** The dependence of the probability of convergence to a definite color state for a single node graph on the number of colors. Three machines are shown: the coherent Ising machine (CIM) [10] and based on the triangular [22] and  $V_2$  models.

with a definite color. For the triangular model [22], Fig. 3 shows the outcome of optimally rounding the nonbinary terminal state. The coherent Ising machine (CIM) [10] was simulated using package `cim_optimizer` [26]. The performance of CIM depends on the choice of hyperparameters. We evaluated the sets of values of hyperparameters provided in the package documentation and found that, for the considered problem, the default choice yields the best results, which are shown in Fig. 3.

### 3.1 Graph coloring

A proper (node) graph coloring is an assignment of colors to the graph nodes without adjacent nodes bearing the same color. The minimum number of colors needed for proper coloring of graph  $\mathcal{G}$  is called the graph chromatic number,  $\chi_{\mathcal{G}}$ . Finding the chromatic number of a graph from a sufficiently rich family of graphs is an NP-hard problem [27]. Graph coloring may model a limited resource allocation problem, where colors represent the shared resource, nodes play the role of the resource user, and edges denote the potential conflict arising from the simultaneous use of the assigned resource [28, 29]. Real-world applications that can be naturally formulated in terms of the graph coloring problem include job-scheduling on machines where a set of jobs (vertices) must be scheduled over a minimum number of time-slots (colors) while excluding the simultaneous use of time-slots (edges) [30]. Another example is the problem of channel allocation in dense wireless networks [31]. In this case, nodes stand for individual devices, colors are associated with the channels, and edges represent the interference due to sharing the same channel.

To apply Ising machines, the  $K$ -coloring problem, when the graph  $\mathcal{G}$  is colored with no more than  $K$  colors, must be formulated as the max-cut problem [6, 32]. A straightforward way to obtain such a formulation is to start by representing the graph coloring by a set of binary variables  $s_{i,\kappa} \in \{0, 1\}$ , where  $i = 1, 2, \dots, N$  enumerate the graph nodes and  $\kappa = 1, 2, \dots, K$  correspond to colors. Consequently,  $s_{i,\kappa}$  serve as state variables:  $s_{i,\kappa} = 1$  if the  $i$ -th node is assigned color  $\kappa$ , and  $s_{i,\kappa} = 0$  otherwise. Thus,

for given node  $i$ , the collection of binary variables  $s_{i,\kappa}$  represents a one-hot encoding of the assigned color.

The cost function characterizing the coloring comprises two components. The first component aims to make the coloring proper: adjacent vertices must have different colors. This condition is expressed as  $A_{i,j} \sum_{\kappa} s_{i,\kappa} s_{j,\kappa} = 0$  for all edges  $(i, j) \in E$ . In the optimization context, this amounts to penalizing configurations that do not meet the requirement of proper coloring by  $H^{(1)}(\mathbf{s}) = \sum_{i,j} A_{i,j} \sum_{\kappa} s_{i,\kappa} s_{j,\kappa} / 2$ .

Next, for each node  $i$ , only one of the  $K$  binary variables  $s_{i,\kappa}$  may take the  $+1$  value, which leads to the one-hot encoding constraint  $\sum_{\kappa=1}^K s_{i,\kappa} = 1$ . This constraint can be incorporated by using the Lagrangian relaxation when configurations violating the constraint are assigned a penalty  $H^{(2)}(\mathbf{s}) = \sum_i \left( \sum_{\kappa=1}^K s_{i,\kappa} - 1 \right)^2$  incorporated into the cost function with the respective Lagrange multiplier  $\lambda$ . Thus,  $K$ -coloring is found as found by solving an optimization problem: finding the minimum of the cost function  $H(\mathbf{s}) = H^{(1)}(\mathbf{s}) + \lambda H^{(2)}(\mathbf{s})$ .

To solve the  $K$ -coloring problem using the  $V_2$ -machine, the problem is reformulated in terms of the native to the model spin variables  $\sigma \in \{\pm 1\}$ , using the substitution  $s_{i\kappa} = (\sigma_{i\kappa} + 1)/2$ . This yields the penalty associated with colliding colors

$$H^{(1)}(\boldsymbol{\sigma}) = \frac{1}{2} \sum_{i,j} A_{i,j} \left( \sum_{\kappa} \sigma_{i,\kappa} \sigma_{j,\kappa} + 2 \sum_{\kappa} \sigma_{i,\kappa} \sigma_0 \right), \quad (11)$$

and the one-hot encoding constraint,  $\sum_{\kappa} \sigma_{i,\kappa} = 2 - K$ ,

$$H^{(2)}(\boldsymbol{\sigma}) = \sum_{i,\kappa,\gamma} \sigma_{i,\kappa} \sigma_{i,\gamma} + 2(K-2) \sum_{i,\kappa} \sigma_{i,\kappa} \sigma_0. \quad (12)$$

In Eqs. (11) and (12), we have introduced an auxiliary spin  $\sigma_0 \equiv 1$ , which ensures that the cost function is quadratic in spin variables. Collecting these contributions together, we obtain the spin formulation of the graph coloring problem

$$\boldsymbol{\sigma}' = \arg \min_{\boldsymbol{\sigma}} \left( H^{(1)}(\boldsymbol{\sigma}) + \lambda H^{(2)}(\boldsymbol{\sigma}) \right). \quad (13)$$

Equations (11), (12), and (13) reveal an important structure of the formulation of the  $K$ -coloring problem for the Ising machines. The coloring penalty,  $H^{(1)}(\boldsymbol{\sigma})$ , after constructing the relaxation following the procedure outlined in Section 2, yields the dynamics of spins on graph  $\mathcal{G} \times \mathcal{K}_K$ , a tensor product of the original graph  $\mathcal{G}$  and the complete graph  $\mathcal{K}_K$  describing the one-hot encoding constraint, with an added apex, a node connected to all other nodes. In turn,  $H^{(2)}(\boldsymbol{\sigma})$  produces the dynamics resulting in the emergence of valid colors on  $N$  disconnected complete graphs  $\mathcal{K}_K$  with apexes.

For writing the equations of motion governing the  $V_2$  machine, it is convenient to introduce a homogeneous enumeration of the variables across the auxiliary spin and the tensor product of graph nodes and color encoding sets using  $\alpha, \beta \in \{0, 1, \dots, NK\}$  corresponding to  $\{0, (1, 1), (1, 2), \dots, (N, K)\}$ . Using this enumeration, the penalty



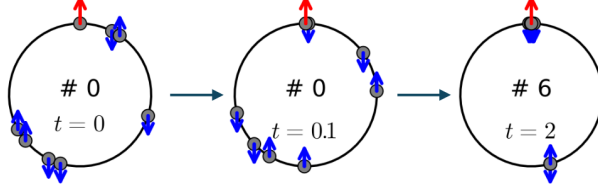


**Fig. 4** An example of the progression of a spin complex representing  $K = 7$  colors from an initial generic state to a state with definite color. The stationary red vertical arrow shows the auxiliary spin. The label at the center shows the identified color (0 corresponds to the state that does not represent a valid color). Shown time is measured in units of the equations of motion [Eq. (16)].

terms  $H^{(k)}(\boldsymbol{\sigma})$ , with  $k = 1, 2$ , can be written as quadratic forms,  $H^{(k)}(\boldsymbol{\sigma}) = \boldsymbol{\sigma}^T \widehat{A}^{(k)} \boldsymbol{\sigma}$ , with the adjacency matrices

$$\widehat{A}^{(1)} = \begin{pmatrix} 0 & K \mathbf{e}_{NK} \\ K \mathbf{e}_{NK}^T & \widehat{A}_{\mathcal{G}} \times \widehat{I}_K \end{pmatrix}, \quad \widehat{A}^{(2)} = \begin{pmatrix} 0 & (K-2) \mathbf{e}_{NK} \\ (K-2) \mathbf{e}_{NK}^T & \widehat{I}_N \times \widehat{A}_{\mathcal{K}} \end{pmatrix}, \quad (14)$$

where  $\mathbf{e}_{NK} = (1, \dots, 1)$  is a vector with  $NK$  unit components,  $\widehat{I}_M$  is the  $M \times M$  identity matrix,  $\widehat{A}_{\mathcal{G}}$  and  $\widehat{A}_{\mathcal{K}}$  are the adjacency matrices of graphs  $\mathcal{G}$  and  $\mathcal{K}_K$ , respectively, and  $\widehat{A} \times \widehat{B}$  denotes the Kronecker product of matrices  $\widehat{A}$  and  $\widehat{B}$ .

The respective relaxed forms of the penalty terms defining the dynamics of the  $V_2$  machine are  $H_V^{(k)}(\boldsymbol{\sigma}, \mathbf{X}) = H^{(k)}(\boldsymbol{\sigma}) + \widetilde{H}_V^{(k)}(\boldsymbol{\sigma}, \mathbf{X})$ , where

$$\widetilde{H}_V^{(k)}(\boldsymbol{\sigma}, \mathbf{X}) = \frac{1}{4} \sum_{\alpha, \beta} A_{\alpha, \beta}^{(k)} \sigma_{\alpha} \sigma_{\beta} |X_{\alpha} - X_{\beta}|. \quad (15)$$

The separated dynamics structure is reflected by the respective equations of motion

$$\dot{\mathbf{X}} = -\nabla_{\mathbf{X}} \widetilde{H}_V^{(1)}(\boldsymbol{\sigma}, \mathbf{X}) - \lambda \nabla_{\mathbf{X}} \widetilde{H}_V^{(2)}(\boldsymbol{\sigma}, \mathbf{X}), \quad (16)$$

where the negative sign denotes that the machine evolves towards the minimum of the penalty, and the coordinate of the auxiliary spin is kept fixed  $\dot{X}_0 \equiv 0$ .

### 3.2 Emergence of definite color states

The separated form of equations of motion (16) allows us to pose the problem of the emergence of the states corresponding to definite colors. The dynamics of individual nodes toward the definite color states is governed by  $H_V^{(2)}(\boldsymbol{\sigma}, \mathbf{X})$ , which is independent for different nodes. Therefore, to investigate the emergence of definite colors, it suffices to consider this dynamics for graph  $\mathcal{K}_{K+1}$  corresponding to coloring of a one-node graph. In this case, the dominant factor determining the dynamics of the spin variables in the spin complex is their interaction with the auxiliary spin owing to the relatively large weight of the respective coupling. Considering the dynamics represented on a circle with circumference 2, generally, “free” spins co-oriented with the auxiliary spin are repelled from it, while counter-oriented ones are attracted, as illustrated by Fig. 4.

**Theorem 1.** *The only stable equilibrium states of the  $V_2$  dynamics of the spin complexes representing a color are states with definite color.*

*Proof.* The theorem statement follows from the general property of the  $V_2$  model established in [24]: for any weighted graph  $\mathcal{G}$ , only states  $(\boldsymbol{\sigma}, \mathbf{X})$  with  $\boldsymbol{\sigma}$  yielding the maximum cut partition of  $\mathcal{G}$  are stable equilibria.

In turn, inspecting the definition of  $H^{(2)}(\boldsymbol{\sigma})$ , one can see that the definite color states correspond to the maximum cut of the graph with the adjacency matrix given by  $\hat{A}^{(2)}$ . It is, however, constructive to show this directly. We notice that graph  $\mathcal{K}_{K+1}$  described by the adjacency matrix  $\hat{A}^{(2)}$  is obtained from  $\mathcal{K}_K$  with edges of unit weight by adding an apex (the auxiliary spin) connected with the  $\mathcal{K}_K$  by edges with weight  $K - 2$ . Thus, graph  $\mathcal{K}_{K+1}$  is symmetric with respect to permutations of the nodes of the “underlying” graph  $\mathcal{K}_K$ . Therefore, the weight of the cut of graph  $\mathcal{K}_{K+1}$  is determined only by the number of positive and negative spins on graph  $\mathcal{K}_K$ .

Let the part of spin configuration  $\boldsymbol{\sigma}$  have of  $\mathcal{K}_K$  spins  $U \geq 0$  and  $D \geq 0$  number of spins equal to  $+1$  and  $-1$ , respectively ( $U + D = K$ ). Then, the cut of graph  $\mathcal{K}_{K+1}$  produced by  $\boldsymbol{\sigma}$  has the weight

$$C_{K+1}(\boldsymbol{\sigma}) = D(K - 2) + UD, \quad (17)$$

where the first term is the weight of cut apex edges, and the second term is the weight of cut of the  $\mathcal{K}_K$  edges. It is straightforward to check that  $C_{K+1}(\boldsymbol{\sigma})$  reaches maximum  $\bar{C}_{K+1} = (K - 1)^2$  at  $U = 1$ , that is a definite color state.  $\square$

Identifying stable equilibria is not sufficient for describing the terminal states of the  $V_2$  machine, as, starting from a generic initial state, the machine may terminate in a saddle critical point of  $H_V^{(2)}(\boldsymbol{\sigma}, \mathbf{X})$ . To explain the high probability of convergence demonstrated in Fig. 4, we need more refined description of the equilibria.

We take into account that, as shown in [24], equilibria of the  $V_2$ -machine on any weighted graph  $\mathcal{G}_W = \{\mathcal{V}_W, \mathcal{E}_W\}$  have the form of strong clustered states  $(\boldsymbol{\sigma}, \mathbf{X})$ , with the set of nodes  $\mathcal{V}_W$  partitioned into  $R(\boldsymbol{\sigma})$  (the order of the state) disjoint subsets according to  $\mathcal{V}_W = \bigcup_p \mathcal{V}^{(p)}$ , where  $\mathcal{V}^{(p)} = \{v \in \mathcal{V}_W : X_u = X^{(p)}\}$  and  $1 \leq p \leq R(\boldsymbol{\sigma})$ . As was shown in [24], the state order is bounded from above by the degeneracy of the binary configuration  $\boldsymbol{\sigma}$  defined as the number of graph partitions with the same cut weight as produced by  $\boldsymbol{\sigma}$ .

To consider perturbed equilibria, we need to extend the notion of clustered states beyond strong clusters. To this end, we assume that the set  $\{X^{(p)}\}$  characterizing the equilibrium state is covered by nonoverlapping *open* intervals  $(X_-^{(p)}, X_+^{(p)})$  such that the set of nodes is partitioned between  $\mathcal{V}^{(p)} = \{v \in \mathcal{V}_W : X_u \in (X_-^{(p)}, X_+^{(p)})\}$  and all  $\mathcal{V}^{(p)}$  are non-empty.

Due to the symmetry discussed in the proof of Theorem 1, the matrix elements of  $\hat{A}^{(2)}$  can be presented for  $\alpha \neq 0$  as  $A_{\alpha, \beta}^{(2)} = q_\beta$  with  $q_0 = K - 2$  and  $q_\beta = 1$  for  $\beta > 0$ . Using this representation and the weak cluster partitioning, the equations of motion

can be written in a form

$$\dot{X}_\alpha = \frac{1}{2} \sum_{\beta \in \mathcal{V}^{(p)}} q_\beta \sigma_\alpha \sigma_\beta \operatorname{sgn}(X_\alpha - X_\beta) + \frac{\sigma_\alpha \bar{Q}^{(p)}}{2}, \quad (18)$$

where we have introduced  $\bar{Q}^{(p)} = \sum_{q < p} Q^{(q)} - \sum_{q > p} Q^{(q)}$ , a charge external to cluster  $\mathcal{V}^{(p)}$  determined by the charge associated with the clusters

$$Q^{(q)} = \sum_{\beta \in \mathcal{V}^{(q)}} q_\beta \sigma_\beta. \quad (19)$$

We note that, as follows from Theorem 1, the only stable equilibria of spin complexes representing colors are the equilibria with clusters of zero total charge.

It is evident that the necessary condition for the (strong) clustered state characterized by  $\{X^{(p)}\}$  to be an equilibrium is for the external charge to vanish:  $\bar{Q}^{(p)} = 0$ , for all  $p$ . This gives a simple criterion for describing all equilibrium states of spin complexes representing a color.

**Theorem 2.** *Equilibrium states of the  $V_2$ -machine driven by  $H_V^{(2)}(\boldsymbol{\sigma}, \mathbf{X})$  have orders  $1 \leq R \leq 3$ .*

*Proof.* The case  $R = 1$ , when  $X_\alpha = 0$  for  $\alpha = 0, \dots, K$ , is trivial as the right-hand-side of Eq. (18) vanishes identically.

For  $R > 1$ , the condition of vanishing external charges,  $\bar{Q}^{(p)} = 0$ , for all  $p$ , has the form of a system of homogeneous equations with respect to cluster charges, or, in other words, an equation for eigenvectors corresponding to the zero eigenvalue of an antisymmetric  $R \times R$  matrix with all the elements below the main diagonal equal to 1. Subtracting the  $(p-1)$ -th row, with  $p > 1$ , of the matrix from the  $p$ -th row, we obtain the relation between the charges of successive clusters:  $Q^{(p)} = (-1)^p Q^{(1)}$ . Adding the first and the last rows yields the ‘‘boundary condition’’  $Q^{(R)} = Q^{(1)}$ .

It follows then that for the even orders, the system with respect to cluster charges admits only trivial solutions,  $Q^{(p)} = 0$ . At the same time, the cluster containing the auxiliary spin may have zero charge only when it contains  $K - 2$  spins with values  $-1$ . Thus, there may be only two clusters, and, therefore, the only equilibrium states of even order are with  $R = 2$  with the same structure. All but two relaxed spin variables have (for  $\alpha > 0$ )  $\sigma_\alpha = -1$  and  $X_\alpha = 0$ . The remaining two variables form a separate cluster with  $\sigma_\beta = -\sigma_{\beta'} = 1$  and  $X_\beta = X_{\beta'} \in [-1, 1] \setminus \{0\}$ . Index  $\beta$  yields the color represented by the spin complex. Together with the case  $X_\beta = 0$  (that is an  $R = 1$  state), this gives an explicit construction of all stable equilibrium states from Theorem 1.

For equilibrium states of odd order with  $R > 1$ , we only need to consider non-trivial solutions to  $\bar{Q}^{(p)} = 0$ , for all  $p$ . The strongest constraint imposed on these solutions is that the magnitude of cluster charges must be equal to the charge of the cluster containing the auxiliary spin. A simple counting argument shows that this constraint may only be satisfied with no more than three clusters. This leaves only possible  $R = 3$

for equilibrium states. All such states have the same structure: all but four relaxed spin variables have (for  $\alpha > 0$ )  $\sigma_\alpha = -1$  and  $X_\alpha = 0$  yielding the cluster with a charge equal to the magnitude of the total state charge,  $\left| \sum_p Q^{(p)} \right| = 2$ . The remaining four variables are split between two clusters,  $\{\beta_1, \beta'_1\}$  and  $\{\beta_2, \beta'_2\}$ , with  $\sigma_{\beta_k} = \sigma_{\beta_{k'}}$  and  $X_{\beta_k} = X_{\beta_{k'}}$ . The signs of the spins depend on the mutual ordering between 0,  $X_{\beta_1}$  and  $X_{\beta_2}$ . Such states exist for problems with  $K \geq 4$ .  $\square$

The structure of charged equilibrium states (with  $R = 1$  or  $R = 3$ ) has a characteristic feature: they contain high-charge ( $Q > 1$ ) sub-clusters with coinciding  $X$  coordinates of the constituting variables. Considering the dynamics of two close co-oriented relaxed spins using the weak cluster partitioning and Eqs. (18), one can see that such sub-clusters cannot form dynamically and must be present in the initial conditions. Therefore, it can be concluded that almost all generic initial states terminate in a stable equilibrium state.

It must be noted, however, that these results hold for formal equations of motion. In particular implementations employing various approximations for solving the equations of motion, there may be specific factors impacting the convergence of the machine. For example, in the present paper, in particular, to obtain results presented in Fig. 3, we have used the Euler approximation. It is exact outside of the hyperplanes where two or more relaxed spin variables have the same  $X$  coordinates. However, when the system phase point traverses these hyperplanes, the Euler approximation leads to various spurious oscillations. The oscillations affecting the convergence to definite color states occur when two co-oriented relaxed spins change signs within the same time step. It can be seen that such a situation may occur when the two-node cluster in an  $R = 2$  equilibrium state is formed within the interval  $\Delta X = \Delta t$  containing the  $X = \pm 1$  point, where  $\Delta t$  is the approximation time-step. Since the position of the two-node cluster is not restricted by general dynamical properties, the probability of such an event can be estimated as  $\sim \Delta t/2$ . In turn, due to the general constraint  $\Delta t \ll 2$ , the probability of encountering such spurious states is small, which is reflected in Fig. 3. There are different techniques for breaking the formation of spurious oscillations near the  $X = \pm 1$  point while generally staying within the Euler approximation. A detailed analysis of improved algorithms for solving equations of motion governing the  $V_2$ -machine [Eq. (7) with  $\phi_V = \phi_R$ ] is beyond the scope of the present paper and will be provided elsewhere.

The last that needs commenting on is how the results discussed above manifest in the context of solving of the graph coloring problem. The relation between the coloring optimization and the convergence to the definite color in the equations of motion is governed by the Lagrange multiplier. Generally,  $\lambda$  needs to be carefully chosen so that each component is not too low while the other is too high, creating an unfavorable bias towards one of the requirements imposed on the machine terminal state. It is, therefore, important that the transition from an equilibrium to a non-equilibrium state creates a “restoring force” (the variation of the contribution of the second term in Eq. (16)) with the magnitude of at least  $\lambda$ . Hence, if the magnitude of the perturbation in Eq. (16) due to the coloring term does not exceed  $\lambda$ , the machine’s behavior is governed by Theorems 1 and 2. Since for the problems regarded here, the

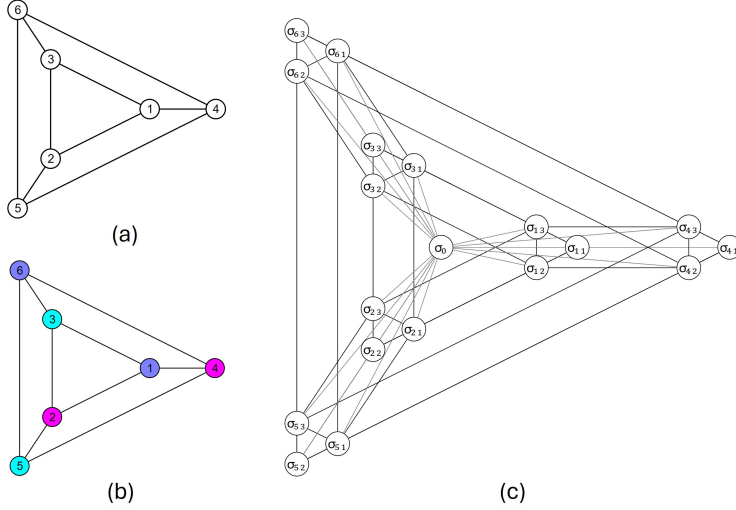


**Fig. 5** Example coloring problem. (a) 6-node problem graph; (b) possible coloring of the 6-node graph; (c) Ising model of the graph, the central node in the graph is the auxiliary node with the fixed spin.

perturbation vanishes when the coloring is found, taking  $\lambda = 1$ , as was done in our studies discussed below, is sufficient. A more complete description of the strategies for choosing the correct value of  $\lambda$  is a subject of ongoing research.

### 3.3 Example of a proper graph coloring using the $V_2$ model

Next, we illustrate the solution of graph coloring problem using the  $V_2$  model. Figures 5a and 5b show the example graph  $\mathcal{G}$  with  $\chi_{\mathcal{G}} = 3$  chosen for the illustration and an example of its proper coloring. As described above, the problem graph of Fig. 5a is transformed into a max-cut problem graph (or an Ising graph) that has the form of  $\mathcal{G} \times \mathcal{K}_3$  supplied with an apex as shown in Fig. 5c. Each node of the Ising graph is labeled as  $\sigma_{i,\kappa}$ , where  $i$  is the node index in the original graph and  $\kappa$  is the index of the color. The weight of the edge between nodes  $\sigma_{i,\kappa}$  and  $\sigma_{j,\kappa}$

$$w(\sigma_{i,\kappa}, \sigma_{j,\kappa}) = 1, \quad (20)$$

and between  $\sigma_{i,\kappa}$  and  $\sigma_{i,\mu}$

$$w(\sigma_{i,\kappa}, \sigma_{i,\mu}) = \lambda. \quad (21)$$

The auxiliary node connects to all nodes of the Ising graph with a uniform weight

$$w_{0,(i,\kappa)} = \lambda + 3. \quad (22)$$

Figure 6a plots the evolution of  $\xi$  with time and demonstrates that the  $V_2$  machine solves the coloring problem without converging to a binary state. As pointed out before, this is in contrast with the existing machines such as in [15, 33].

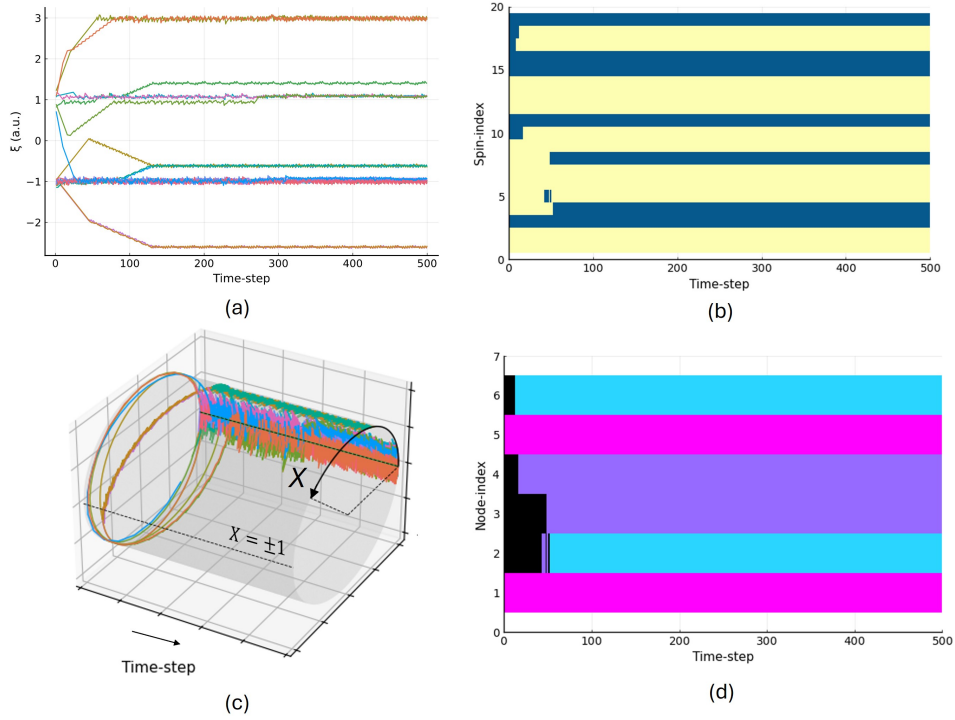


**Fig. 6** Dynamical progression for the example coloring problem. (a)  $\xi$ -evolution in  $V_2$  model; (b) spin-evolution (green implying spins state of ‘1’); (c) evolution of the continuous component,  $X$ ; (d) Color assignment based on the spins. Black regions indicate spin configurations that do not correspond to any color as they violate the one-hot color encoding constraint.

The evolution of the relaxed spins (the  $(\sigma, X)$  representation) is depicted in Figs. 6b and 6c, with the  $X$  coordinates plotted on a cylinder  $[-1, 1) \times \text{time}$  with the apparent formation of the clusters characteristic for equilibrium states of the  $V_2$  dynamics. The consequence of the finite time-step of the employed Euler approximation is the spurious oscillations near the positions of the (true) strong clusters, similar to the oscillations discussed above.

The evolution of color, derived from the spin evolution, is plotted in Fig. 6d. Black strips indicate the absence of valid color assignment for that node. Thus, we see that the  $V_2$  model successfully solves the coloring problem of the selected graph by providing sufficiently good solutions to the corresponding max-cut problem, especially so that each vertex is assigned one (and only one) color. In contrast, the coloring of slightly larger planar graphs on CIM was shown to require developing a special multi-stage procedure involving a regular adjustment of adjacency matrix [34].

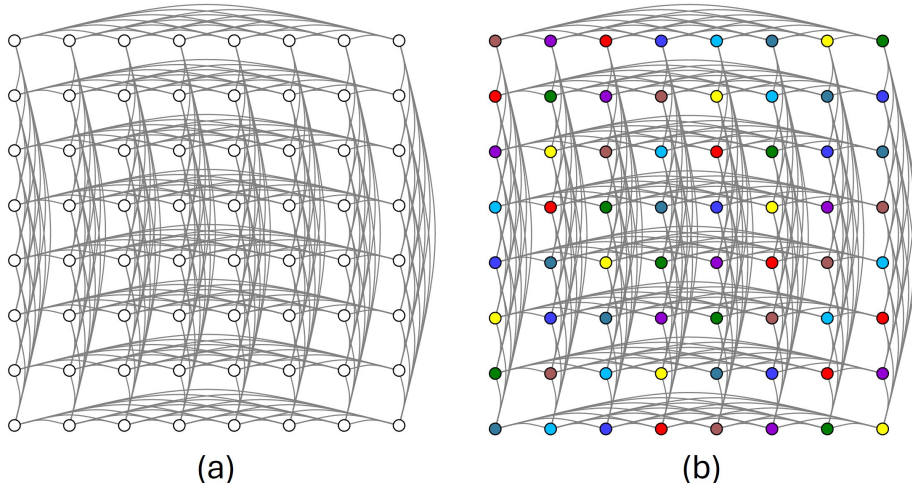


**Fig. 7** Latin square/rook's graph. (a)  $8 \times 8$  uncolored; (b)  $8 \times 8$  colored graph

## 4 Latin squares and the Sudoku puzzle

A Latin square is an  $N \times N$  (square) array of  $N$  distinct labels arranged so that each row and column of the square has all the  $N$  labels exactly once, without repetitions or omissions. The number of such arrangements is known to grow super-exponentially with  $N$  [35], although an expression allowing for an efficient evaluation of the number of Latin squares is unknown [36]. Latin squares are primarily used in statistical designs (for example, maximizing soil utility in agriculture), error-correcting codes, and potentially, at larger scales, cryptography [37].

Constructing an  $N \times N$  Latin square is equivalent to the  $N$ -coloring of a graph whose vertices correspond to cells of the square and edges connect vertices belonging to the same row or column, or the size- $N$  rook's graph (Fig. 8a) [38]. As the most basic test of the applicability of  $V_2$  model in larger scale combinatorics, we apply it to the coloring of the  $8 \times 8$  rook's graph.

Figure 8a shows the evolution of  $\xi$  for the Ising model of the rook's graph using the  $V_2$  dynamics when  $\xi$  is randomly initialized. Most features of its evolution are the same as for the example coloring problem. In addition, we see an initial flux in the machine state, with relatively larger increments arising from a generally larger density of the graph. Throughout this flux, a well-defined, albeit suboptimal, binary state vector is always available. The evolution of  $\xi$  reaches a “noisy” steady state composed of clusters whose thickness depends on the time-discretization parameter and the typical degree of a node, as discussed above.

Figures 8b and 8c show the evolution of the spin state,  $\sigma(t)$  and the continuous component  $\mathbf{X}(t)$ , respectively. Here, the period of  $\xi$  flux ( $T < 100$ ) translates into the similar period of  $\mathbf{X}$ -flux where it evolves the fastest and actively traverses its range, and terminates such that all  $X$  settle in a cluster centered at 0.



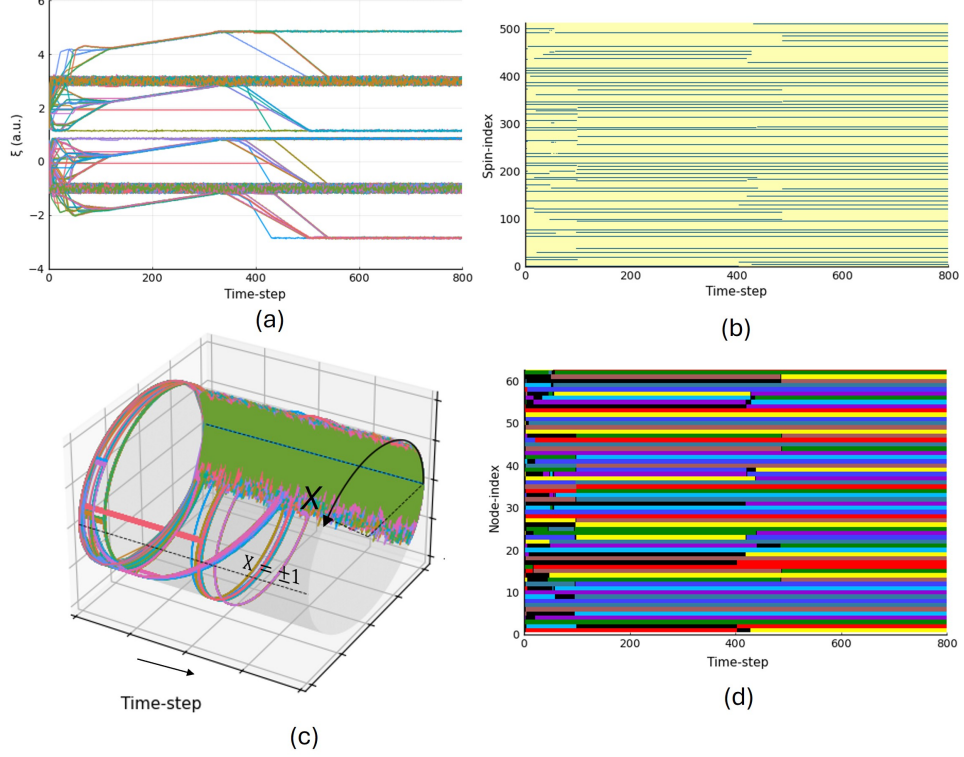


**Fig. 8** Dynamical progression for the coloring of rook's graph. (a)  $\xi$ -evolution in  $V_2$  dynamics; (b) spin-evolution (green implying spins state of '1'); (c)  $X$ -evolution; (d) Color assignment based on the spins. Black indicates the intervals when the machine state does not yield a valid color.

Progression of the color assignment from the  $V_2$  model is shown in Fig. 8d, where black regions correspond to the time intervals when the spin component  $\sigma$  violates the one-hot encoding constraint, that is when no valid color can be assigned. The result of the coloring of the rook's graph is shown in Fig. 7b.

Next, we apply the  $V_2$  model to solve the popular combinatorics puzzle Sudoku. This numeric puzzle can be regarded as set on a Latin square (Fig. 9a) but with additional constraints. Besides the prohibited repetitions of labels within individual rows and columns, the labels must be unique within predefined regions on the square. The canonical Sudoku puzzle is set on a  $m^2 \times m^2$  grid with the predefined regions being  $m \times m$  sub-squares. Finally, the puzzle is formulated by providing clues: pre-filling some cells with labels (Fig. 9b-c). For a  $9 \times 9$  puzzle to be well-posed, that is to have a unique solution, at least 17 clues must be provided. Similar to how a Latin square was found in the previous section, the Sudoku grid can be filled by coloring the Sudoku graph depicted in Fig. 9d, whereas solving Sudoku puzzles requires coloring partially colored graphs.



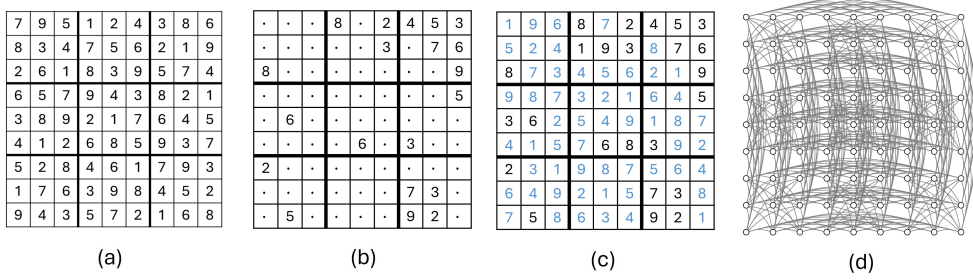


**Fig. 9** Elements of the Sudoku puzzle. (a)  $9 \times 9$  Sudoku grid with a valid arrangement of the digits 1 to 9; (b) an example of the Sudoku puzzle; (c) solved Sudoku puzzle; (d) 81-node Sudoku graph.

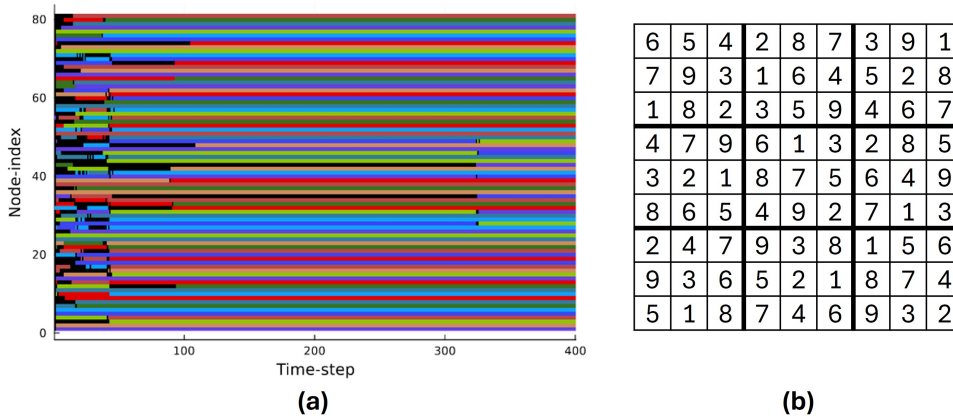


**Fig. 10** Filling up the Sudoku grid using the  $V_2$ -machine. (a) Evolution of color assigned to the individual cells; (b) The final state of the Sudoku grid.

For  $V_2$ -machine programmed to fully color the graph in Fig. 9d, Fig. 10 shows the evolution of colors in the machine and Fig. 10b shows the Sudoku grid at the end of the dynamics. The same machine successfully solves the first 50 standard Sudoku Kaggle puzzles available at [39]. Figure 11a shows the puzzle we consider for illustration. Figure 11b shows the evolution of color, starting from a coloring corresponding to the puzzle in Fig. 11a, and Fig. 11c shows the solution of the puzzle.

## 5 Conclusion

The growing interest in alternative models of computing has revived the Ising models as the basis for accelerated as well as scaled combinatorial optimization. All NP-hard problems can be recast in terms of the problem of ground-state search of the Ising model and solved on realizations of the Ising model called Ising machines.

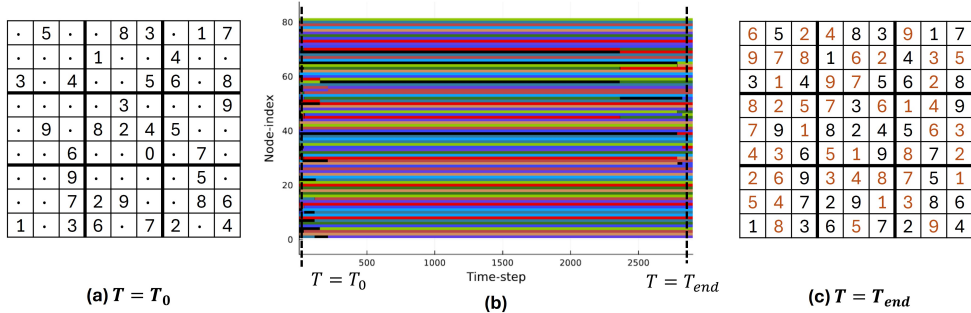


**Fig. 11** Solving Sudoku puzzle. (a) Sudoku puzzle. Coloring corresponding to the clues (at  $T = T_0$ ) are held constant throughout the dynamics; (b) Color evolution; (c) Solution square as obtained from the coloring at  $T = T_{end}$ .

A new class of dynamical Ising machines, implemented on a variety of computing platforms, approach the search problem from the theoretical dynamical systems perspective by redefining the problem in terms of continuous spins and delivering the solution via its terminal state. At the same time, the discrete nature of combinatorics puts tight constraints on the output (or the terminal state) of these dynamics. Since the Ising model is based on binary spins, variables of dynamical Ising machines must ultimately correspond to binary values. Hence, the dynamical Ising machine, on the one hand, relies on the continuity of spins to be effective at navigating the energy landscape and, on the other, must terminate at states composed of binary spins.

The  $V_2$  model sets itself apart from the current dynamical Ising machines in that it does not put forth such requirements and is allowed to converge to a highly non-binary state. The relation between the non-binary states of the  $V_2$  machine and, by requirement, the binary form of a sought solution is straightforwardly established by a hybrid binary-continuous representation (the relaxed spin). The key property of the  $V_2$  model is that the spin configuration contained in the binary component of the relaxed spin representation in the machine's terminal state is of the same quality as an optimal rounding of the underlying non-binary state.

As applications of the Ising machines to realistic problems are being gradually expanded, concerted research effort is needed to develop Ising models of such problems and establish these machines' efficacy at solving a diverse set of foundational problems. We demonstrate the computational capabilities of the non-binary dynamical Ising machine based on the  $V_2$  model through the coloring of non-planar complex graphs, namely those corresponding to Latin squares and the Sudoku puzzle. Importantly, we show that the  $V_2$  model inherently converges to states satisfying the feasibility constraint (definite color). This property signifies the applicability of the Ising machine based on the  $V_2$  model to a broad class of high-level optimization problems where the feasibility requirement is critical for the sole mapping of the problem to an Ising machine.

## References

- [1] Kirkpatrick, S., Gelatt, C. D. & Vecchi, M. P. Optimization by Simulated Annealing. *Science* **220**, 671–680 (1983).
- [2] Hopfield, J. J. Neurons with graded response have collective computational properties like those of two-state neurons. *Proceedings of the National Academy of Sciences* **81**, 3088–3092 (1984).
- [3] Černý, V. Thermodynamical approach to the traveling salesman problem: An efficient simulation algorithm. *Journal of Optimization Theory and Applications* **45**, 41–51 (1985).
- [4] Fu, Y. & Anderson, P. W. Application of statistical mechanics to NP-complete problems in combinatorial optimisation. *Journal of Physics A: Mathematical and General* **19**, 1605–1620 (1986).
- [5] Barahona, F. On the computational complexity of Ising spin glass models. *Journal of Physics A: Mathematical and General* **15**, 3241–3253 (1982).
- [6] Lucas, A. Ising formulations of many NP problems. *Frontiers in Physics* **2**, 1–14 (2014). URL <http://journal.frontiersin.org/article/10.3389/fphy.2014.00005/abstract>.
- [7] Mohseni, N., McMahon, P. L. & Byrnes, T. Ising machines as hardware solvers of combinatorial optimization problems. *Nature Reviews Physics* **4**, 363–379 (2022).
- [8] Bybee, C. *et al.* Efficient optimization with higher-order Ising machines. *Nature Communications* **14**, 6033 (2023). URL <https://www.nature.com/articles/s41467-023-41214-9>.
- [9] Si, J. *et al.* Energy-efficient superparamagnetic Ising machine and its application to traveling salesman problems. *Nature Communications* **15**, 3457 (2024). URL <https://www.nature.com/articles/s41467-024-47818-z>.
- [10] Yamamoto, Y. *et al.* Coherent Ising machines—optical neural networks operating at the quantum limit. *npj Quantum Information* **3**, 49 (2017).
- [11] Zhang, Y., Afoakwa, R., Vengalam, U. K. R., Huang, M. & Ignjatovic, Z. A CMOS Compatible Bistable Resistively-coupled Ising Machine-BRIM. *Proceedings - IEEE International Symposium on Circuits and Systems* **2022-May**, 1665–1669 (2022).
- [12] Böhm, F., Vaerenbergh, T. V., Verschaffelt, G. & Van der Sande, G. Order-of-magnitude differences in computational performance of analog Ising machines induced by the choice of nonlinearity. *Communications Physics* **4**, 149 (2021).
- [13] Marandi, A., Wang, Z., Takata, K., Byer, R. L. & Yamamoto, Y. Network of time-multiplexed optical parametric oscillators as a coherent Ising machine. *Nature Photonics* **8**, 937–942 (2014). URL <http://www.nature.com/articles/nphoton.2014.249>.
- [14] Leleu, T., Yamamoto, Y., Utsunomiya, S. & Aihara, K. Combinatorial optimization using dynamical phase transitions in driven-dissipative systems. *Physical Review E* **95**, 4–6 (2017).
- [15] Goto, H., Tatsumura, K. & Dixon, A. R. Combinatorial optimization by simulating adiabatic bifurcations in nonlinear Hamiltonian systems. *Science Advances* **5**, 1–9 (2019).
- [16] Shukla, A., Erementchouk, M. & Mazumder, P. Custom CMOS Ising Machine

- Based on Relaxed Burer-Monteiro-Zhang Heuristic. *IEEE Transactions on Computers* **72**, 2835–2846 (2023). URL <https://ieeexplore.ieee.org/document/10187692/>.
- [17] Wang, T., Wu, L. & Roychowdhury, J. New Computational Results and Hardware Prototypes for Oscillator-based Ising Machines. In *Proceedings of the 56th Annual Design Automation Conference 2019*, vol. 2, 1–2 (ACM, New York, NY, USA, 2019). URL <https://dl.acm.org/doi/10.1145/3316781.3322473>.
- [18] Erementchouk, M., Shukla, A. & Mazumder, P. On computational capabilities of Ising machines based on nonlinear oscillators. *Physica D: Nonlinear Phenomena* **437**, 133334 (2022). URL <https://arxiv.org/abs/2105.07591><https://linkinghub.elsevier.com/retrieve/pii/S0167278922001075>.
- [19] Bashar, M. K., Lin, Z. & Shukla, N. Stability of oscillator Ising machines: Not all solutions are created equal. *Journal of Applied Physics* **134**, 144901 (2023). URL <https://doi.org/10.1063/5.0157107>. [https://pubs.aip.org/aip/jap/article-pdf/doi/10.1063/5.0157107/18161910/144901\\_1\\_5.0157107.pdf](https://pubs.aip.org/aip/jap/article-pdf/doi/10.1063/5.0157107/18161910/144901_1_5.0157107.pdf).
- [20] Williamson, D. P. & Goemans, M. Improved Maximum Approximation Algorithms for Using Cut and Satisfiability Programming Problems Semidefinite. *Science* **42**, 1115–1145 (1994).
- [21] Burer, S., Monteiro, R. D. & Zhang, Y. Rank-two relaxation heuristics for MAX-CUT and other binary quadratic programs. *SIAM Journal on Optimization* **12**, 503–521 (2002).
- [22] Shukla, A., Erementchouk, M. & Mazumder, P. Scalable almost-linear dynamical Ising machines. *Natural Computing* (2024). URL <http://arxiv.org/abs/2205.14760><https://link.springer.com/10.1007/s11047-024-09983-4>.
- [23] Punnen, A. P. (ed.) *The Quadratic Unconstrained Binary Optimization Problem* (Springer International Publishing, Cham, 2022). URL <https://link.springer.com/10.1007/978-3-031-04520-2>.
- [24] Erementchouk, M., Shukla, A. & Mazumder, P. Self-contained relaxation-based dynamical Ising machines (2023). URL <https://arxiv.org/abs/2305.06414>.
- [25] Garey, M. R. & Johnson, D. S. *Computers and Intractability; A Guide to the Theory of NP-Completeness* (W. H. Freeman & Co., 1990).
- [26] Chen, F. *et al.* cim-optimizer: a simulator of the Coherent Ising Machine (2022). URL <https://github.com/mcmahon-lab/cim-optimizer>.
- [27] Karp, R. M. Reducibility among Combinatorial Problems. In *Complexity of Computer Computations*, 85–103 (Springer US, Boston, MA, 1972). URL [http://link.springer.com/10.1007/978-1-4684-2001-2\\_9](http://link.springer.com/10.1007/978-1-4684-2001-2_9).
- [28] Hale, W. K. Frequency Assignment: Theory and Applications **68** (1980).
- [29] Boev, A. S. *et al.* Quantum-inspired optimization for wavelength assignment. *Frontiers in Physics* **10**, 1–11 (2023).
- [30] Leighton, F. A graph coloring algorithm for large scheduling problems. *Journal of Research of the National Bureau of Standards* **84**, 489 (1979). URL [https://nvlpubs.nist.gov/nistpubs/jres/84/jresv84n6p489\\_A1b.pdf](https://nvlpubs.nist.gov/nistpubs/jres/84/jresv84n6p489_A1b.pdf).
- [31] Wu, K. J., Hong, Y. W. & Sheu, J. P. Coloring-Based Channel Allocation for Multiple Coexisting Wireless Body Area Networks: A Game-Theoretic Approach. *IEEE Transactions on Mobile Computing* **21**, 63–75 (2022).

- [32] Glover, F., Kochenberger, G. & Du, Y. Quantum Bridge Analytics I: a tutorial on formulating and using QUBO models. Tech. Rep. 4 (2019). URL <https://leeds-faculty.colorado.edu/glover/511-QUBOTutorial-updatedversion-May4,2019.pdf>.
- [33] Inagaki, T. *et al.* A coherent Ising machine for 2000-node optimization problems. *Science* **354**, 603–606 (2016). URL <https://www.sciencemag.org/lookup/doi/10.1126/science.aah4243>.
- [34] Inaba, K. *et al.* Potts model solver based on hybrid physical and digital architecture. *Communications Physics* **5**, 1–8 (2022).
- [35] Van Lint, J. H. & Wilson, R. M. *A Course in Combinatorics* (Cambridge University Press, 1992).
- [36] Stones, D. S. The Many Formulae for the Number of Latin Rectangles. *The Electronic Journal of Combinatorics* **17** (2010). URL <https://www.combinatorics.org/ojs/index.php/eljc/article/view/v17i1a1>.
- [37] Colbourn, C. J. & Dinitz, J. H. (eds.) *Handbook of Combinatorial Designs* (Chapman and Hall/CRC, 2006). URL <https://www.taylorfrancis.com/books/9781420010541>.
- [38] Laskar, R. & Wallis, C. Chessboard graphs, related designs, and domination parameters. *Journal of Statistical Planning and Inference* **76**, 285–294 (1999). URL <https://linkinghub.elsevier.com/retrieve/pii/S0378375898001323>.
- [39] Park, K. 1 million Sudoku games (2016). URL <https://www.kaggle.com/datasets/bryanpark/sudoku>.